Sudden freshening and cooling of western North Atlantic slope water at the onset of the Little Ice Age based on Magnesium-to-Calcium ratio and oxygen stable isotope record.

Wai Ching Rachel Chu[1,2], Tiffany Audet[3], Anne de Vernal[3], Benoit Thibodeau[1,*]

[1]Department of Earth and Environmental Sciences & School of Life Sciences, The Chinese University of Hong Kong, Sha Tin, N.T., Hong Kong S.A.R, China.

[2]Now at School of Ocean and Earth Science, Faculty of Environmental and Life Sciences, University of Southampton, Southampton, SO17 1BJ, United Kingdom.

[3]GEOTOP, Université du Québec à Montréal, Montréal, Québec, Canada.

*Corresponding author:

Email address: benoit.thibodeau@cuhk.edu.hk (B. Thibodeau).

ABSTRACT

The Little Ice Age (LIA, ~1400–1850 CE) was characterized by colder winters and more frequent extreme weather events in the Northern Hemisphere. While changes in ocean circulation likely contributed to global cooling, the specific mechanisms remain poorly understood. Here, we investigate how ocean circulation changed before, during, and after the LIA using marine sediment cores from the Laurentian Channel in the Lower St. Lawrence Estuary. We first established a Mg/Ca-temperature calibration for *Globobulimina auriculata* using instrumental temperature data and a century-old box core. Applying this calibration to a longer piston core, we reconstructed bottom-water temperatures during the LIA. Coupling these results with existing $\delta^{18}O$ calcite data allowed us to isolate the $\delta^{18}O$ seawater signal, which reflects changes in the relative contributions of the Labrador Current and Gulf Stream. Our results indicate an increase of fresh and cold Labrador Sea-derived waters around 1500 CE. Throughout most of the LIA we observed a slow and steady warming of the bottom water associated with a gradual increase in the proportion of Atlantic-derived waters until ~1850 CE. The ~1800–1950 CE interval shows high-amplitude variability, including a sudden freshening event at the LIA's end. After 1950 CE, regional warming dominates, consistent with previous studies documenting increased Atlantic influence over the Canadian shelf.

KEYWORDS

Mg/Ca ratio, foraminifera, oxygen isotope, St Lawrence Estuary, temperature reconstruction, Little Ice Age, Labrador Current, Gulf Stream, AMOC, Paleoceanography

1. INTRODUCTION

The Little Ice Age (LIA) is a relatively short climate anomaly (~1400-1850 CE, with variable onset timing depending on the region), was characterized by abrupt cooling and glacier expansion, following the warming in Medieval Climate Anomaly (MCA) (Brönnimann et al., 2019; Wanner et al., 2022). The LIA is the coldest period in the last 8,000 years, being 0.7 to 1°C cooler in the Northern Hemisphere than in the 2000 CE (Lean and Rind, 1999). It is also associated with a higher frequency of extreme weather and more extreme seasonal temperatures. Due to the higher land coverage, the Northern Hemisphere was suggested to be more affected than the Southern Hemisphere (Wanner et al., 2022). The socio-economic impacts of the LIA have been relatively well documented (e.g., Behringer 1999; Fan 2023; Putnam et al. 2016), making it a valuable period for understanding how abrupt climate change may affect our livelihoods. It also provides valuable insights into ocean-climate interactions as its late occurrence provided us with relatively high resolution in the sedimentary records. While the dominating factors causing the onset of LIA are still not fully resolved, previous studies suggest that sea ice-ocean and atmosphere-ocean feedbacks may have played a significant role (e.g., Moffa-Sánchez et al., 2019).

One key part of the ocean-climate feedback is the Atlantic Meridional Overturning Circulation (AMOC), which is a branch of the thermohaline circulation in the North Atlantic Ocean (Broecker et al., 1985; Stommel, 1961), The Gulf Stream and the Labrador Current are two major ocean currents that play key roles in the AMOC and in shaping the dynamics of the North Atlantic subtropical and subpolar gyres. (Figure 1). The Gulf Stream is a northeastward-flowing warm surface current originating in the Gulf of Mexico, bringing heat

up the meridians, while the Labrador Current is a cold surface current flowing southward along the North Atlantic coast under the Coriolis force. Their respective strengths have been used to assess changes in the AMOC strength across different intervals, such as the Holocene and modern times (Ezer, 2015; Rashid et al., 2017; Thibodeau et al., 2018, 2010). While the strength of the AMOC has experienced large amplitude variations during Earth's history, slight variations are often overlooked, which may be as informative about the potential consequences of global warming for the AMOC (Galaasen et al., 2020; Thibodeau et al., 2025).

During the LIA, changes in the subpolar gyre and/or AMOC may have impacted meridional heat transport to higher latitudes, thereby influencing the climate of the North Atlantic and subpolar regions (e.g., Moffa-Sánchez et al., 2014). Multiple studies have attempted to characterize changes in AMOC and identify its drivers during this period (Table S1); two different mechanisms have been proposed to explain changes in AMOC, i.e., wind forcing and freshwater forcing. In the wind forcing scenario, it was suggested that the negative North Atlantic Oscillation caused weaker northwestern wind and more frequent Southern wind, leading to a weaker Labrador Current and associated northward shift in the Gulf Stream (Jutras et al., 2023; Sicre et al., 2014), thus resulting in a weaker AMOC. On the other hand, in the freshwater forcing scenario, the increase in storminess (Dawson et al., 2007) during LIA led to more sea ice formation, break-off, and rafting, which eventually melted and contributed to the Labrador Current. The large quantity of freshwater decreased the salinity, lowering the density gradient and thus weakening Labrador Sea convection and the subpolar gyre convection, resulting in a decrease in AMOC (Alonso-Garcia et al., 2017; Holliday et al., 2020; Moffa-Sánchez et al., 2014; Moffa-Sánchez and Hall, 2017; Rashid et al., 2023;

Thibodeau et al., 2018, 2010; Thornalley et al., 2018).

Previous reconstructions of northwestern Atlantic oceanography have described a sharp cooling from the MCA to the LIA (Keigwin, 1996) and a progressive increase in the relative contribution of Atlantic-derived water in the Laurentian Channel toward the end of the LIA, as evidenced by oxygen isotope records from benthic foraminifera (Thibodeau et al. 2018). More recent work also suggested a gradual replacement of Labrador-derived water throughout the LIA based, again, on $\delta^{18}O_{calcite}$ measurements and end-member mixing calculations (Keigwin et al., 2025). However, disentangling the temperature and $\delta^{18}O_{seawater}$ solely from the $\delta^{18}O_{calcite}$ is complex and relies on a set of assumptions, notably the consistency of the endmembers over time. One way to elucidate the $\delta^{18}O_{seawater}$ from the $\delta^{18}O_{calcite}$ is to reconstruct temperature, which is possible from measurements of magnesium-to-calcium ratio .

The magnesium-to-calcium ratio (Mg/Ca) in perforate foraminiferal tests is governed by both biological processes (Bentov and Erez, 2006; Erez, 2003) and the physicochemical properties of ambient seawater (Alkhatib et al., 2022; Katz, 1973; Mucci, 1987; Rosenthal et al., 1997). Since both are strongly temperature-dependent, Mg/Ca serves as a widely used paleothermometer (e.g., Elderfield and Ganssen, 2000). The solubility of calcite decreases with increasing temperature (Segnit et al., 1962), and more Mg^{2+} is incorporated into inorganically precipitated calcite with increasing temperature. Temperature also enhances ATP hydrolysis, the chemical process that converts ATP to ADP and releases energy. Since ATP molecules can bind free Mg^{2+} ions, enhanced ATP hydrolysis results in less ATP available and thus fewer Mg^{2+} ions to be bound by ATP. This process increases the

concentration of free Mg^{2+} ions in the cellular environment, thus increasing the Mg/Ca ratio (Bentov and Erez, 2006; Romani and Maguire, 2002). Another factor governing the Mg/Ca ratio in calcite is the diffusion constant of Mg^{2+} ions, which increases with temperature, facilitating diffusion between ambient seawater and the vacuole of the foraminifers (Bentov and Erez, 2006).

The Laurentian Channel serve as a recorder of NW Atlantic subsurface conditions due to its depth of about 350m (Thibodeau et al., 2010). The proportion of Labrador Subarctic Slope Water (LSSW) versus Atlantic Temperate Slope Water (ATSW) entering the Laurentian Channel is primarily controlled by the strength of the northern recirculation gyre (Hogg et al., 1986), which itself depends on the intensity of deep water formation in the Labrador Sea and the associated deep western boundary current (Zhang et al., 2007). When Labrador Sea convection is vigorous and the AMOC is strong, the recirculation gyre keeps the Gulf Stream path well separated from the coast, allowing greater southward penetration of cold, oxygen-rich LSSW along the continental shelf edge and into the Laurentian Channel (Thibodeau et al., 2018). Conversely, during periods of weak convection — characteristic of modern conditions — the recirculation gyre weakens, the Gulf Stream shifts northward, and a larger proportion of warm, oxygen-poor ATSW enters the channel. This mechanism explains why the proportion of LSSW in the Laurentian Channel bottom water decreased from approximately 72% to 53% over the twentieth century, driving a bottom water warming of about 1.7 °C that is ultimately linked to the ongoing weakening of the AMOC (Thibodeau et al., 2018; Thornalley et al., 2018).

In this paper, we used in-solution ICP-MS measurements from individual foraminifer tests to

establish a Mg/Ca-temperature calibration curve for *Globobulimina auriculata* in the lower St. Lawrence Estuary. By removing the temperature signal from published oxygen isotopic data, we then reconstructed the relative proportions of Labrador Current and Atlantic water entering the Laurentian Channel to better understand the dynamics of these water masses during the LIA. We thus aim to provide new insights into oceanographic changes in the NW Atlantic during the LIA and thus contribute to a better understanding of the relationship between AMOC, the subpolar gyre, and climate.

2. METHODOLOGY

2.1 Sediment core and subsampling

Two sediment cores obtained from the St. Lawrence Estuary were used for this study (Figure S1). Core CR02-23 is a 0.12 m^2 x 0.5 m long and was collected at 48º42.008'N, 68º38.894'W at 345m, during an expedition of the *R/V Coriolis II* in 2002 CE. The age-depth model of the core was previously established using Pb-210 (Thibodeau et al., 2018, 2010, 2006). A 1.8-yr age uncertainty was calculated in the age model (Figure S2). Five cm^3 of wet sediment was taken at 1-cm intervals from 0 to 30 cm, with an additional sampling at 0.5 cm depth. The depth corresponded to 1933 – 2001 CE. The average sediment rate was 0.42 cm/yr. Analyses of this CR02-23 core were used to establish a Mg/Ca–temperature calibration equation.

Core MD99-2220 is 51.6 m long and was collected at 48°38.32N, 68°37.93W, at 320 m of water depth during an expedition of the *R/V Marion Dufresne* in 1999. The upper 14 cm of the core was missing due to handling disturbances (St-Onge et al., 2003). The lithostratigraphy of the core had been divided into two units, Unit 1 from the base of the core to 1497 cm), and Unit 2 from 1497 cm to the surface. Unit 1 consists of grey to dark grey laminated to massive clays, while Unit 2 consists of postglacial bioturbated silty clay (St-

Onge et al., 2003). The age-depth model was established using radiocarbon dating (St-Onge et al., 2003), with a 2σ uncertainty of ±100 yr. For our study of the LIA interval, 5 cm^3 of wet sediment was taken from the core at 1-cm intervals from 0 cm to 75.5 cm, with an additional sample at 0.5 cm depth. The study interval spans from 1396 to 1975 CE, which covers the LIA (Figure S2). According to the age model of St-Onge et al. (2003), sedimentation rates are approximately 0.74 cm/yr for the upper 20 cm, 0.28cm/yr from 20 to 30 cm, and 0.15 cm/yr from 30 to 75 cm (Figure S2).

For all sample, wet sediment was sieved through a 63-μm mesh sieve to remove silt and clay. In the coarse fraction (>125μm), foraminifera were examined under the Leica EZ4W Stereomicroscope, and adult specimens of *Globobulimina auriculata* were identified and hand-picked. In most samples, four intact foraminifer shells were selected from each depth as replicates (Trejos et al., 2003).

2.2 Cleaning

The tests were cleaned according to the protocol of Barker et al. (2003), but without the reductive cleaning step to remove the Mn-oxide coatings (Martin and Lea, 2002). Previous studies observed a 10-15% Mg/Ca ratio decrease after reductive cleaning (Barker et al., 2003; Martin and Lea, 2002). However, only a 0.03 mmol/mol (i.e., ~1%) decrease in Mg/Ca is expected if all Mn-Fe oxide coating is removed (Barker et al., 2003). Given that the Mg/Ca ratio in this foraminifer species is low, averaging 3.65 mmol/mol, we did not perform a reductive cleaning step to avoid excessive Mg/Ca loss.

2.3 Single-foraminifer ICP-MS Analysis

All measurements were performed using an Agilent 7900 ICP-MS at the Chinese University of Hong Kong. We used JCp-1, a certified coral reference material developed by the Geological Survey of Japan commonly used for other foraminiferal studies (e.g. Zhou et al., 2022; Yoshimura et al., 2011), as an internal standard. A self-made multi-element solution (MeRC) was served as a reference material, comprising a mixture of pure Ca, Mg, Sr, Mn, and Fe solutions and 2% nitric acid. The accuracy and precision of JCp-1 and MeRC were measured multiple times every run with ICP-MS and were consistently within 5% of expected values, if not the samples were run again if possible. Each run of the ICP-MS analysis was composed of 2% nitric acid blank acquisition at the start and end of the run. Every five foraminiferal sample acquisitions were accompanied by a set of reference material and 2% nitric acid blank for recalibration and brief cleaning of the machine. Details of the ICP-MS setup are reported in the supplementary information.

Raw data were obtained from the ICP-MS Data Analysis window software (Agilent Technologies, 2014). Because ICP-MS can be relatively unstable, frequent recalibration of the instrument against reference materials is required (Jackson and Sylvester, 2008). Re-calibration was done with MeRC correction, in which the cps of each elemental isotope in the first MeRC acquisition of each run was used as the baseline. These baseline cps values were then compared against the subsequent MeRC acquisitions within the same run. Variations between MeRC acquisition and the baseline were computed to define the linear slope. The samples in between acquisitions were corrected with the respective slope. To mitigate the effects of omitting a reductive cleaning step, data exceeding the elimination thresholds determined from our location data were considered contaminated and removed (see Table S2).

2.3.1 CR02-23 Calibration Curve and Temperature Reconstruction Comparison

The downcore comparison of MeRC-corrected $^{24}Mg/^{48}Ca$ data and instrumental temperature compiled by Thibodeau et al. (2010), led to the establishment of our calibration curves, which was tested with both linear fit and exponential fit. The $^{24}Mg/^{48}Ca$ data led to the reconstruction of the bottom water temperature (*t in Celsius*), and were compared using the following calibration equations:

Eq.1) Lear et al. (2002), which used benthic foraminifera belonging to *Cibicidoides* from core-tops:

$$Mg/Ca\ (mmol/mol) = (0.867 \pm 0.049)\ e^{((0.109 \pm 0.007)t)}$$

Eq.2) Weldeab et al. (2016), which used the genus *Globobulimina*:

$$Mg/Ca\ (mmol/mol) = (0.36\ \pm 0.02)t + 2.22 \pm 0.19$$

2.3.2 Salinity Effect

The salinity impact on the Mg/Ca ratio in foraminifera is under debate, especially for benthic foraminifera (e.g. Mathien-Blard and Bassinot 2009; Weldeab, Arce, and Kasten 2016). To investigate the effect of salinity on our Mg/Ca data, two approaches were used. 1) Mg/Ca data were analysed against the instrumental salinity data at 300 m depth in the study area (Galbraith et al., 2018); 2) Differences between our Mg/Ca data and back-calculated Mg/Ca from the Weldeab et al. (2016) equation in *Globobulimina* (Eq.2) were compared against instrumental salinity.

2.4 MD99-2220 Parent Water Mass Reconstruction

The calibration curve from the core CR02-23 Mg/Ca data was applied to reconstruct bottom-water temperature from core MD99-2220. Using the $\delta^{18}O_{(calcite)}$ data previously obtained for MD99-2220 (Thibodeau et al., 2018), we could calculate the $\delta^{18}O_{(seawater)}$ signal from the equation of Marchitto et al. (2014), which assumes a 0.9‰ offset for vital effect as measured for *Globobulimina affinis* (Hoogakker et al., 2010):

$$t\ (^{o}\ C) = \frac{0.245 - \sqrt{0.045461 + 0.0044(\ \delta^{18}O\ _{(calcite)} - \delta^{18}O\ _{(seawater)})}}{0.0022}$$

Given that the Atlantic Temperate Slope Water (ATSW) and Labrador Sea Slope Water (LSSW) have distinct $\delta^{18}O$ signals, we can track the change of contribution from $\delta^{18}O_{(seawater)}$ changes (Thibodeau et al. 2018, 2010). In the $\delta^{18}O_{(seawater)}$ reconstruction, a positive signature represents a dominant ATSW (proxy for Gulf Stream) and a negative signature represents a dominant LSSW (proxy for Labrador Current). A 95% confidence interval was applied for all statistical analyses, and all results were corrected to two decimal places, apart from cps, R-squares, and equations. All analyses and graphs were produced on GraphPad Prism 9.0 and Excel, while maps were produced via the use of Ocean Data View.

3. RESULT

3.1 CR02-23

In core CR02-23, measurements were made in a total of 75 samples of foraminifera. All elemental isotopes measured exceeded the limits of detection (LOD) and quantification (LOQ), indicating quantifiable concentrations.

3.1.1 Mg/Ca Ratio

After applying the elimination threshold (Table S2), 43 measurements remained for analysis. The $^{24}Mg/^{48}Ca$ ranges from 1.72 to 9.01 mmol/mol (Table S3). The p-value for the linear

regression model of isotope ratios was < 0.05, representing a significant relationship between bottom water temperature and Mg/Ca ratio (Figure 2a). For both linear and non-linear (exponential) models, the R-squared values were > 0.7, indicating a significant correlation between temperature and the Mg/Ca ratio (Table S4). The exponential equation is chosen because it yielded a higher R-squared (R^2=0.76) than that of the linear model (R^2=0.74).

3.1.2 Salinity Effect and Contamination

No statistically significant relationship was observed between salinity and Mg/Ca (p-value >0.05, R-square <0.02; Figure 2b and Table S5). However, the lack of correlation could result from the small sample size (n=8) and the narrow salinity range (32.34 to 34.94 psu). No significant correlation was observed between Mn/Ca or Fe/Ca with Mg/Ca (Figure 3). A low but significant correlation was observed between Al/Ca and Mg/Ca, suggesting minimal contamination.

3.2 MD99-2220

A total of 286 foraminiferal samples were analysed. After applying the elimination threshold, 100 measurements remained for data analysis.

The average Mg/Ca ratio in MD99-2220 across depths 0 cm to 76 cm ranged from 1.14 to 9.16 mmol/mol. Reconstruction yielded bottom-water temperatures of 1.58-7.18°C (Figure 4a). We observed a stepwise increase in temperature from ~1396 to 1905 CE, followed by a decrease from ~1905 CE onwards with large fluctuations in the 20th century. The seawater isotope signal declined from the base of the record until ~1500 CE, then increased stepwise until ~1800 CE, after which a sharp decrease was recorded (Figure 4b). Because of the

relatively high standard deviation of our measurements, we remained cautious when discussing small-amplitude variations in our record.

4. DISCUSSION

4.1 Calibration of Mg/Ca vs temperature in the St. Lawrence Estuary

4.1.1 Comparisons of Calibrations

We compared the CR02-23 Mg/Ca ratio with previously established calibrations for temperature estimates from Mg/Ca, thereby testing the applicability of published equations (Lear et al., 2002; Weldeab et al., 2016) for *G. auriculata* at our study location. The temperature reconstructions using published equations yield a wide range of values (-1 to 28 °C), well outside the study environment's range (3 to 6 °C). This highlights the need for a regional calibration curve using *Globobulimina auriculata.*

4.1.2 Calibration Equation for Globobulimina auriculata in the Lower St. Lawrence Estuary

The calibration equation was established as the best-fit exponential equation from $^{24}Mg/^{48}Ca$ data after MeRC correction and instrumental temperature from the St. Lawrence bottom water (Thibodeau et al., 2018):

$$Mg/Ca\ (mmol/mol) = 0.6341e^{(0.3740t)}$$

where t represents water temperature in Celsius

This equation yielded a range of bottom-water temperatures of 3.0 to 5.5°C, with an R-square of 0.76 between instrumental and estimated values. It is important to note that this calibration used Mg/Ca values from the sediment core and instrumental temperature records on a calendar-year scale. Therefore, the correlation may be affected by uncertainty in the core

chronology. Moreover, because we used the local temperature gradient over time, the calibration covers only a 3 °C temperature range. While this calibration can provide a fine-scale reconstruction, the narrow temperature range may have amplified uncertainty in the relationship between the actual and reconstructed data, resulting in a relatively low coefficient of correlation. Finally, assuming that carbonate ion concentration mainly affects the Mg/Ca ratio at bottom-water temperatures < 3 °C (Elderfield et al. 2006), we did not account for the effect of carbonate ion, which may be an additional caveat. Regardless of these potential limitations, the calibration equation tailored to *Globobulimina auriculata* in the Lower St. Lawrence Estuary appears robust for regional reconstructions of temperature through time. However, it is important to note that the most recent part of the record includes data that are outside our calibration range, which may explain the higher variability observed, notably in the most recent part of the cores where temperatures are expected to be warmer.

4.2 Little Ice Age temperature reconstruction

Changes in bottom-water temperature reconstructed from our Mg/Ca data followed a pattern similar to our expectation based on literature, namely a cooling at the beginning of the LIA following by a gradual warming throughout the LIA (Figure 4a) (e.g., Forman et al., 2025; Keigwin, 1996; Keigwin et al., 2025; Thibodeau et al., 2018). Our calculated $\delta^{18}O_{seawater}$ was characterized by similar pattern than the temperature (Figure 4b) supporting previous interpretation suggesting that the dominant factor controlling temperature changes is likely related to the mixing proportions of parent water masses in the bottom water of the lower St. Lawrence Estuary.

Non-parametric Mann-Kendall Trend Test was applied to identify significant trends. A positive trend characterized the ~1490 to ~1850 CE interval for both $\delta^{18}O_{seawater}$ and

323 temperature (Table S6). Transitions were thus identified at 1490 and 1850 CE, yielding three
324 time-intervals in the study sequence (Figure 5), which are discussed hereafter with reference
325 to potential drivers of change in the dynamics of western North Atlantic circulation during
326 the LIA. This segmentation is aligned with previous studies suggesting the onset of the LIA
327 in this region to be around 1500 CE (e.g., Keigwin et al., 2025).

328

329 *4.2.1 Transition from MCA to LIA (pre 1500 CE)*

330 This time interval was characterized by a relatively constant signal, followed by a relatively
331 sharp decrease in both temperature and seawater $\delta^{18}O$ in the latter half of the 15th century
332 suggesting increased influence of Labrador-derived water at our site. This cooling is
333 synchronous with an increase in the size of sortable silt from Southeast Grand Banks,
334 suggesting an increase in Labrador Current flow speed since ~1450 CE (Rashid et al., 2023),
335 before the rise in the contribution of LSSW as reconstructed herein. This may have been
336 caused by an increase freshwater transport into the Labrador Sea slope waters as suggested
337 by modern observational data (Lazier and Wright, 1993). Increased freshwater release in the
338 Labrador Sea has been reconstructed for the LIA, which may originate from meltwater
339 produced during the warm Medieval Climate Anomaly (MCA) (Alonso-Garcia et al., 2017;
340 Lapointe and Bradley, 2021; Moffa-Sánchez et al., 2014). This freshwater discharge has been
341 observed from TEX_{86}-T and higher presence of Polar waters at Eirik Drift (Rashid et al.,
342 2023). These evidences also aligns with relatively cool condition in the Sargasso Sea
343 (Keigwin, 1996) and relatively low $\delta^{18}O$, indicating fresh and cold condition, in the Jordan
344 Basin (Keigwin et al., 2025) This explains the cooling observed from ~1470 CE in our core
345 (Figure 4a), and the higher presence of stronger Labrador Sea current-derived waters (Figure
346 4b). This is also coherent with a weaken Gulf stream (Caesar et al., 2018; Rahmstorf et al.,

2015), and reduced northward heat transport (Lund et al., 2006) reducing the relative contribution of the ATSW as estimated from our record (Figure 4).

4.2.2 The Little Ice Age (~1500 to 1850 CE)

In the study region, the LIA was characterized by a significant increasing trend of oxygen isotope signature and bottom water temperature (Table S6). The coldest and freshest subsurface water in the Labrador Sea was recorded right at the beginning of the 16th century, as indicated by our Mg/Ca ratios, which is coherent with $\delta^{18}O$ values in *Neogloboquadrina pachyderma* (Moffa-Sánchez et al., 2014). Gradually during the LIA, more saline waters were observed until around 1800 CE (Lund et al., 2006) and can be attributed to drier conditions in the West Atlantic (Saenger et al., 2011). The increased salinity of the Gulf Stream, resulting in a higher oxygen isotope composition of the ATSW, might have contributed to the rise in $\delta^{18}O_{seawater}$ in our reconstruction (Figure 4b).

The end of LIA (~1810-1850 CE) coincides with the early stage of the industrial era (~1830 CE onwards), during which air temperature and sea surface temperature recorded a <0.2 °C and <0.5 °C increase, respectively (Abram et al., 2016). However, climate-related warming cannot account for the ~2 °C increase observed in bottom water temperature. (Figure 5) Therefore, we hypothesize that the regional warming was mainly caused by the enhanced contribution of ATSW relative to LSSW. The timing of the peak matched the end of the large-scale ice-rafting events in ~1800 CE (Alonso-Garcia et al., 2017) and the end of the series of volcanic eruptions (~1835 CE) (Brönnimann et al., 2019). A decrease in the deep western boundary current (DWBC) was also inferred from sortable silt (Thornalley et al., 2018), which may reduce the amount of $\delta^{18}O$-depleted water reaching this site and thus explains the

maximum oxygen isotopic signal observed during this interval. This is also consistent with other studies suggesting a gradual northward displacement of the Gulf Stream in the later stage of the LIA (Forman et al., 2025).

4.2.3 Post-LIA (post 1850 CE)

This beginning of this interval has lower resolution, mostly due to contaminated samples, and thus the comparison with other records is not straightforward. Moreover, we observed very high variability, especially in the 20th century. The start of this interval was marked by an important cooling of approximately 3°C of bottom-water temperature between ~1850 CE and ~1925 CE. While this cooling seems to align with a resurgence of LSSW at our site and a strengthening of the AMOC (Figure 5), this cooling is only recorded in two samples and thus should be interpreted with caution. Moreover, this cooling is immediately followed by a 3°C warming between ~1925 CE and ~1934 CE. The following two decades are then characterised by a cooling of about 2.5°C, followed by a similar warming of >2°C in the second half of the 20th century (~1954 CE to the end of our record). Interestingly, the observed cooling at the beginning of this period coincides with a short-lived peak in hematite-stained grain abundance in the Labrador Sea, indicating a sudden and significant increase in Arctic sea-ice export through the Eastern Greenland Current (Alonso-Garcia et al., 2017). Therefore, the drop in $\delta^{18}O_{seawater}$ may be caused by an increase in Labrador-derived water, but also by the freshening of this endmember. The latter could also explain why this cooling seems at odds with other interpretations of regional $\delta^{18}O$ records that suggested a warming from the beginning of the 20th century (Keigwin et al., 2025; Thibodeau et al., 2018). However, a transient cooling of about 2°C was also observed in the Jordan basin deep water with coldest condition around 1920 CE (Keigwin et al., 2025). Moreover, while the

Gulf Stream was strengthening as well after the end of the LIA, its $\delta^{18}O_{seawater}$ also dropped by ~0.3‰ (Lund et al., 2006). Therefore, evidence of lower $\delta^{18}O_{seawater}$ values in both endmembers composing the Laurentian bottom water suggests that the isotopic signal may have been primarily controlled by changes in the isotopic composition of these water masses due to freshwater input following the LIA rather than temperature as suggested by previous studies. In the second half of the 20th century, we reconstructed a 2°C warming, coherent with multiple observations in the region and that was attributed to an increased influence of Atlantic-derived water over the Canadian shelf, which is also present in our reconstruction of seawater $\delta^{18}O$ (Genovesi et al., 2011; Gilbert et al., 2005; Keigwin et al., 2003; Keigwin et al., 2025; Thibodeau et al., 2006, 2010, 2013, 2018).

5. CONCLUSION

In this paper, we used single foraminifer ICP-MS to establish an exponential Mg/Ca-temperature calibration curve for *Globobulimina auriculata* at the Lower St. Lawrence Estuary, i.e. $Mg/Ca\ (mmol/mol) = 0.6341e^{(0.3740t)}$. This bottom-water temperature reconstruction curve applies to a temperature range of 3.0-5.5°C. Despite its narrow temperature range, it provides a species- and region-specific curve for relatively accurate temperature reconstruction in future studies. Using the newly established calibration curve and Mg/Ca data from the MD99-2220 core, we reconstructed the bottom-water temperature in the Lower St. Lawrence Estuary during the LIA. Constrained by $\delta^{18}O_{calcite}$ data, we calculated the change in $\delta^{18}O_{seawater}$ and used it as a proxy for the change in the contribution of the parent water mass. Our results, taken together with previous evidence, indicate that the transition from MCA to LIA was characterized a sharp decrease in temperature and oxygen isotope values, likely due to increased Labrador Sea-derived water. During the LIA, there was an increasing trend in oxygen isotope signal and bottom water temperature, with a shift

from LSSW to ATSW dominance. The post-LIA period began with a sharp decrease in bottom water temperature, followed by a significant warming trend in the late 20th century, attributed to an increased influence of Atlantic-derived water masses over the Canadian continental shelf.

6. AUTHOR CONTRIBUTIONS

Wai Ching Rachel Chu: Methodology, Formal analysis, Investigation, Data Curation, Writing-Original Draft, Writing – Review & Editing, Visualization. **Anne de Vernal:** Resources, Writing – Review & Editing. **Tiffany Audet:** Resources, Writing – Review & Editing. **Benoit Thibodeau:** Conceptualization, Resources, Data Curation, Visualization, Supervision, Project administration, Funding acquisition, Writing – Review & Editing.

7. DATA AVAILABILITY

Data produced for this paper are available at https://doi.org/10.48668/HLKYYR.

8. ACKNOWLEDGEMENT

This study was funded through the General Research Fund from the Research Grant Council of Hong Kong (#17301320) awarded to Benoit Thibodeau. The sampling and study of marine sediment cores MD99-2220 and CR02-23 were enabled thanks to the support of the Natural Science and Engineering Research Council (NSERC) of Canada and the *Fonds de Recherche du Québec – Nature et Technologie* (FRQNT). The authors thank the technical support provided by Mr Cho On Thomas Tang from the Chinese University of Hong Kong for his help troubleshooting the Agilent 7900 ICP-MS.

9. DECLARATION OF COMPETING INTEREST

Declaration of Interest Statement

The authors declare that they have no known competing financial interests or personal relationships that could have appeared to influence the work reported in this paper.

10. REFERENCES

Abram, N.J., McGregor, H.V., Tierney, J.E., Evans, M.N., McKay, N.P., Kaufman, D.S., 2016. Early onset of industrial-era warming across the oceans and continents. Nature 536, 411–418. https://doi.org/10.1038/nature19082

Agilent Technologies, 2014. Agilent 7900 ICP-MS MassHunter Workstation User Guide.

Alkhatib, M., Qutob, M., Alkhatib, S., Eisenhauer, A., 2022. Influence of precipitation rate and temperature on the partitioning of magnesium and strontium in calcite overgrowths. Chemical Geology 599, 120841. https://doi.org/10.1016/j.chemgeo.2022.120841

Alonso-Garcia, M., Kleiven, H. (Kikki) F., McManus, J.F., Moffa-Sanchez, P., Broecker, W.S., Flower, B.P., 2017. Freshening of the Labrador Sea as a trigger for Little Ice Age development. Climate of the Past 13, 317–331. https://doi.org/10.5194/cp-13-317-2017

Barker, S., Greaves, M., Elderfield, H., 2003. A study of cleaning procedures used for foraminiferal Mg/Ca paleothermometry. Geochemistry, Geophysics, Geosystems 4. https://doi.org/10.1029/2003GC000559

Behringer, W., 1999. Climatic Change and Witch-hunting: the Impact of the Little Ice Age on Mentalities. Climatic Change 43, 335–351. https://doi.org/10.1023/A:1005554519604

Bentov, S., Erez, J., 2006. Impact of biomineralization processes on the Mg content of foraminiferal shells: A biological perspective. Geochemistry, Geophysics, Geosystems 7. https://doi.org/10.1029/2005GC001015

Broecker, W.S., Peteet, D.M., Rind, D., 1985. Does the ocean–atmosphere system have more than one stable mode of operation? Nature 315, 21–26. https://doi.org/10.1038/315021a0

Brönnimann, S., Franke, J., Nussbaumer, S.U., Zumbühl, H.J., Steiner, D., Trachsel, M., Hegerl, G.C., Schurer, A., Worni, M., Malik, A., Flückiger, J., Raible, C.C., 2019. Last phase of the Little Ice Age forced by volcanic eruptions. Nat. Geosci. 12, 650–656. https://doi.org/10.1038/s41561-019-0402-y

Caesar, L., Rahmstorf, S., Robinson, A., Feulner, G., Saba, V., 2018. Observed fingerprint of a weakening Atlantic Ocean overturning circulation. Nature 556, 191–196. https://doi.org/10.1038/s41586-018-0006-5

Dawson, A.G., Hickey, K., Mayewski, P.A., Nesje, A., 2007. Greenland (GISP2) ice core and historical indicators of complex North Atlantic climate changes during the fourteenth century: Holocene. Holocene 17, 427–434. https://doi.org/10.1177/0959683607077010

Elderfield, H., Ganssen, G., 2000. Past temperature and δ18O of surface ocean waters inferred from foraminiferal Mg/Ca ratios. Nature 405, 442–445. https://doi.org/10.1038/35013033

Elderfield, H., Yu, J., Anand, P., Kiefer, T., Nyland, B., 2006. Calibrations for benthic foraminiferal Mg/Ca paleothermometry and the carbonate ion hypothesis. Earth and Planetary Science Letters 250, 633–649. https://doi.org/10.1016/j.epsl.2006.07.041

Erez, J., 2003. The Source of Ions for Biomineralization in Foraminifera and Their Implications for Paleoceanographic Proxies. Reviews in Mineralogy and Geochemistry 54, 115–149. https://doi.org/10.2113/0540115

Ezer, T., 2015. Detecting changes in the transport of the Gulf Stream and the Atlantic overturning circulation from coastal sea level data: The extreme decline in 2009–2010 and estimated variations for 1935–2012. Global and Planetary Change 129, 23–36. https://doi.org/10.1016/j.gloplacha.2015.03.002

Fan, K., 2023. The Little Ice Age and the Fall of the Ming Dynasty: A Review. Climate 11, 71. https://doi.org/10.3390/cli11030071

Forman, E.C.G., Baldini, J.U.L., Jamieson, R.A., Lechleitner, F.A., Walczak, I.W., Nita, D.C., Smith, S.R., Richards, D.A., Baldini, L.M., McIntyre, C., Müller, W., Peters, A.J., 2025. The Gulf Stream moved northward at the end of the Little Ice Age. Commun Earth Environ 6, 552. https://doi.org/10.1038/s43247-025-02446-3

Galaasen, E.V., Ninnemann, U.S., Kessler, A., Irvalı, N., Rosenthal, Y., Tjiputra, J., Bouttes, N., Roche, D.M., Kleiven, H. (Kikki) F., Hodell, D.A., 2020. Interglacial instability of North Atlantic Deep Water ventilation. Science 367, 1485–1489. https://doi.org/10.1126/science.aay6381

Galbraith, P.S., Chassé, J., Caverhill, C., Nicot, P., Gilbert, D., Lefaivre, D., Lafleur, C., n.d. Physical Oceanographic Conditions in the Gulf of St. Lawrence during 2017.

Genovesi, L., de Vernal, A., Thibodeau, B., Hillaire-Marcel, C., Mucci, A., Gilbert, D., 2011. Recent changes in bottom water oxygenation and temperature in the gulf of st. Lawrence: Micropaleontological and geochemical evidence. Limnology and Oceanography 56, 1319–1329. https://doi.org/10.4319/lo.2011.56.4.1319

Gilbert, D., Sundby, B., Gobeil, C., Mucci, A., Tremblay, G.H., 2005. A seventy-two-year record of diminishing deep-water oxygen in the St. Lawrence estuary: The northwest Atlantic connection. Limnology and Oceanography 50, 1654–1666. https://doi.org/10.4319/lo.2005.50.5.1654

Hogg, N.G., Pickart, R.S., Hendry, R.M., Smethie, W.J., 1986. The northern recirculation gyre of the gulf Stream. Deep Sea Research Part A, Oceanographic Research Papers 33, 1139–1165. https://doi.org/10.1016/0198-0149(86)90017-8

Holliday, N.P., Bersch, M., Berx, B., Chafik, L., Cunningham, S., Florindo-López, C., Hátún, H., Johns, W., Josey, S.A., Larsen, K.M.H., Mulet, S., Oltmanns, M., Reverdin, G., Rossby, T., Thierry, V., Valdimarsson, H., Yashayaev, I., 2020. Ocean circulation causes the largest freshening event for 120 years in eastern subpolar North Atlantic. Nat Commun 11, 585. https://doi.org/10.1038/s41467-020-14474-y

Hoogakker, B., Elderfield, H., Oliver, K., Crowhurst, S., 2010. Benthic foraminiferal oxygen isotope offsets over the last glacial-interglacial cycle. Paleoceanography 25. https://doi.org/10.1029/2009PA001870

Jackson, S., Sylvester, P., 2008. Calibration strategies for elemental analysis. Signal 10, 100.

Jutras, M., Dufour, C.O., Mucci, A., Talbot, L.C., 2023. Large-scale control of the retroflection of the Labrador Current. Nat Commun 14, 2623. https://doi.org/10.1038/s41467-023-38321-y

Katz, A., 1973. The interaction of magnesium with calcite during crystal growth at 25–90°C and one atmosphere. Geochimica et Cosmochimica Acta 37, 1563–1586. https://doi.org/10.1016/0016-7037(73)90091-4

Keigwin, L.D., 1996. The Little Ice Age and Medieval Warm Period in the Sargasso Sea. Science 274, 1503–1508. https://doi.org/10.1126/science.274.5292.1503

Keigwin, L.D., Petrie, B., Boyle, E.A., 2025. Slope Water Intrusions Onto Canadian Atlantic Continental Shelf During the Past 1800 Years. Paleoceanography and Paleoclimatology 40, e2025PA005183. https://doi.org/10.1029/2025PA005183

Keigwin, L.D., Sachs, J.P., Rosenthal, Y., 2003. A 1600-year history of the Labrador Current off Nova Scotia. Climate Dynamics 21, 53–62. https://doi.org/10.1007/s00382-003-0316-6

Lapointe, F., Bradley, R.S., 2021. Little Ice Age abruptly triggered by intrusion of Atlantic waters into the Nordic Seas. Science Advances 7, eabi8230. https://doi.org/10.1126/sciadv.abi8230

547 Lazier, J.R.N., Wright, D.G., 1993. Annual Velocity Variations in the Labrador Current.
548 Journal of Physical Oceanography.
549 Lean, J., Rind, D., 1999. Evaluating sun–climate relationships since the Little Ice Age.
550 Journal of Atmospheric and Solar-Terrestrial Physics 61, 25–36.
551 https://doi.org/10.1016/S1364-6826(98)00113-8
552 Lear, C.H., Rosenthal, Y., Slowey, N., 2002. Benthic foraminiferal Mg/Ca-paleothermometry:
553 a revised core-top calibration. Geochimica et Cosmochimica Acta 66, 3375–3387.
554 https://doi.org/10.1016/S0016-7037(02)00941-9
555 Lund, D.C., Lynch-Stieglitz, J., Curry, W.B., 2006. Gulf Stream density structure and
556 transport during the past millennium. Nature 444, 601–604.
557 https://doi.org/10.1038/nature05277
558 Martin, P.A., Lea, D.W., 2002. A simple evaluation of cleaning procedures on fossil benthic
559 foraminiferal Mg/Ca. Geochemistry, Geophysics, Geosystems 3, 1–8.
560 https://doi.org/10.1029/2001GC000280
561 Mathien-Blard, E., Bassinot, F., 2009. Salinity bias on the foraminifera Mg/Ca thermometry:
562 Correction procedure and implications for past ocean hydrographic reconstructions.
563 Geochemistry, Geophysics, Geosystems: G3 10.
564 https://doi.org/10.1029/2008GC002353
565 Moffa-Sánchez, P., Hall, I.R., 2017. North Atlantic variability and its links to European
566 climate over the last 3000 years. Nat Commun 8, 1726.
567 https://doi.org/10.1038/s41467-017-01884-8
568 Moffa-Sánchez, P., Hall, I.R., Barker, S., Thornalley, D.J.R., Yashayaev, I., 2014. Surface
569 changes in the eastern Labrador Sea around the onset of the Little Ice Age.
570 Paleoceanography 29, 160–175. https://doi.org/10.1002/2013PA002523
571 Moffa-Sánchez, P., Moreno-Chamarro, E., Reynolds, D.J., Ortega, P., Cunningham, L.,
572 Swingedouw, D., Amrhein, D.E., Halfar, J., Jonkers, L., Jungclaus, J.H., Perner, K.,
573 Wanamaker, A., Yeager, S., 2019. Variability in the Northern North Atlantic and
574 Arctic Oceans Across the Last Two Millennia: A Review. Paleoceanography and
575 Paleoclimatology 34, 1399–1436. https://doi.org/10.1029/2018PA003508
576 Mucci, A., 1987. Influence of temperature on the composition of magnesian calcite
577 overgrowths precipitated from seawater. Geochimica et Cosmochimica Acta 51,
578 1977–1984. https://doi.org/10.1016/0016-7037(87)90186-4
579 Putnam, A.E., Putnam, D.E., Andreu-Hayles, L., Cook, E.R., Palmer, J.G., Clark, E.H., Wang,
580 C., Chen, F., Denton, G.H., Boyle, D.P., Bassett, S.D., Birkel, S.D., Martin-
581 Fernandez, J., Hajdas, I., Southon, J., Garner, C.B., Cheng, H., Broecker, W.S., 2016.
582 Little Ice Age wetting of interior Asian deserts and the rise of the Mongol Empire.
583 Quaternary Science Reviews 131, 33–50.
584 https://doi.org/10.1016/j.quascirev.2015.10.033
585 Rahmstorf, S., Box, J.E., Feulner, G., Mann, M.E., Robinson, A., Rutherford, S.,
586 Schaffernicht, E.J., 2015. Exceptional twentieth-century slowdown in Atlantic Ocean
587 overturning circulation. Nature Climate Change 5, 475–480.
588 https://doi.org/10.1038/nclimate2554
589 Rashid, H., Piper, D.J.W., Lazar, K.B., McDonald, K., Saint-Ange, F., 2017. The Holocene
590 Labrador Current: Changing linkages to atmospheric and oceanographic forcing
591 factors. Paleoceanography 32, 498–510. https://doi.org/10.1002/2016PA003051
592 Rashid, H., Zhang, Z., Piper, D.J.W., Patro, R., Xu, Y., 2023. Impact of Medieval Climate
593 Anomaly and Little Ice Age on the Labrador Current flow speed and the AMOC
594 reconstructed by the sediment dynamics and biomarker proxies. Palaeogeography,

595 Palaeoclimatology, Palaeoecology 111558.
596 https://doi.org/10.1016/j.palaeo.2023.111558
597 Romani, A.M.P., Maguire, M.E., 2002. Hormonal regulation of Mg2+ transport and
598 homeostasis in eukaryotic cells. Biometals 15, 271–283.
599 https://doi.org/10.1023/a:1016082900838
600 Rosenthal, Y., Boyle, E.A., Slowey, N., 1997. Temperature control on the incorporation of
601 magnesium, strontium, fluorine, and cadmium into benthic foraminiferal shells from
602 Little Bahama Bank: Prospects for thermocline paleoceanography. Geochimica et
603 Cosmochimica Acta 61, 3633–3643. https://doi.org/10.1016/S0016-7037(97)00181-6
604 Saenger, C., Came, R.E., Oppo, D.W., Keigwin, L.D., Cohen, A.L., 2011. Regional climate
605 variability in the western subtropical North Atlantic during the past two millennia.
606 Paleoceanography 26. https://doi.org/10.1029/2010PA002038
607 Schlitzer, R., 2018. Ocean Data View, https://odv.awi.de.
608 Segnit, E.R., Holland, H.D., Biscardi, C.J., 1962. The solubility of calcite in aqueous
609 solutions—I The solubility of calcite in water between 75° and 200° at CO2 pressures
610 up to 60 atm. Geochimica et Cosmochimica Acta 26, 1301–1331.
611 https://doi.org/10.1016/0016-7037(62)90057-1
612 Sicre, M.-A., Weckström, K., Seidenkrantz, M.-S., Kuijpers, A., Benetti, M., Masse, G., Ezat,
613 U., Schmidt, S., Bouloubassi, I., Olsen, J., Khodri, M., Mignot, J., 2014. Labrador
614 current variability over the last 2000 years. Earth and Planetary Science Letters 400,
615 26–32. https://doi.org/10.1016/j.epsl.2014.05.016
616 Stommel, H., 1961. Thermohaline Convection with Two Stable Regimes of Flow. Tellus 13,
617 224–230. https://doi.org/10.3402/tellusa.v13i2.9491
618 St-Onge, G., Stoner, J.S., Hillaire-Marcel, C., 2003. Holocene paleomagnetic records from
619 the St. Lawrence Estuary, eastern Canada: centennial- to millennial-scale geomagnetic
620 modulation of cosmogenic isotopes. Earth and Planetary Science Letters 209, 113–
621 130. https://doi.org/10.1016/S0012-821X(03)00079-7
622 Thibodeau, B., de Vernal, A., Hillaire-Marcel, C., Mucci, A., 2010. Twentieth century
623 warming in deep waters of the Gulf of St. Lawrence: A unique feature of the last
624 millennium. Geophysical Research Letters 37. https://doi.org/10.1029/2010GL044771
625 Thibodeau, B., de Vernal, A., Limoges, A., 2013. Low oxygen events in the laurentian
626 channel during the holocene. Marine Geology 346, 183–191.
627 https://doi.org/10.1016/j.margeo.2013.08.004
628 Thibodeau, B., de Vernal, A., Mucci, A., 2006. Recent eutrophication and consequent
629 hypoxia in the bottom waters of the Lower St. Lawrence Estuary:
630 Micropaleontological and geochemical evidence. Marine Geology 231, 37–50.
631 https://doi.org/10.1016/j.margeo.2006.05.010
632 Thibodeau, B., Doherty, J.M., Alonso-García, M., Band, S., González-Lanchas, A., Not, C.,
633 Ren, H., 2025. Upper Ocean Instability in the Subpolar North Atlantic and Its
634 Implications for Deep Water Formation During Interglacials. Paleoceanography and
635 Paleoclimatology 40, e2024PA004935. https://doi.org/10.1029/2024PA004935
636 Thibodeau, B., Not, C., Zhu, J., Schmittner, A., Noone, D., Tabor, C., Zhang, J., Liu, Z.,
637 2018. Last Century Warming Over the Canadian Atlantic Shelves Linked to Weak
638 Atlantic Meridional Overturning Circulation. Geophys. Res. Lett. 45, 12,376-12,385.
639 https://doi.org/10.1029/2018GL080083
640 Thornalley, D.J.R., Oppo, D.W., Ortega, P., Robson, J.I., Brierley, C.M., Davis, R., Hall, I.R.,
641 Moffa-Sanchez, P., Rose, N.L., Spooner, P.T., Yashayaev, I., Keigwin, L.D., 2018.
642 Anomalously weak Labrador Sea convection and Atlantic overturning during the past
643 150 years. Nature 556, 227–230. https://doi.org/10.1038/s41586-018-0007-4

644 Trejos, T., Montero, S., Almirall, J.R., 2003. Analysis and comparison of glass fragments by
645 laser ablation inductively coupled plasma mass spectrometry (LA-ICP-MS) and ICP-
646 MS. Anal Bioanal Chem 376, 1255–1264. https://doi.org/10.1007/s00216-003-1968-0
647 Wanner, H., Pfister, C., Neukom, R., 2022. The variable European Little Ice Age. Quaternary
648 Science Reviews 287, 107531. https://doi.org/10.1016/j.quascirev.2022.107531
649 Weldeab, S., Arce, A., Kasten, S., 2016. Mg/Ca-ΔCO3porewater2−–temperature calibration
650 for Globobulimina spp.: A sensitive paleothermometer for deep-sea temperature
651 reconstruction. Earth and Planetary Science Letters 438, 95–102.
652 https://doi.org/10.1016/j.epsl.2016.01.009
653 Yoshimura, T., Tanimizu, M., Inoue, M., Suzuki, A., Iwasaki, N., Kawahata, H., 2011. Mg
654 isotope fractionation in biogenic carbonates of deep-sea coral, benthic foraminifera,
655 and hermatypic coral. Anal Bioanal Chem 401, 2755–2769.
656 https://doi.org/10.1007/s00216-011-5264-0
657 Zhang, R., Vallis, G.K., Fluid, G., Oceanic, N., Program, O.S., 2007. The Role of Bottom
658 Vortex Stretching on the Path of the North Atlantic Western Boundary Current and on
659 the Northern Recirculation Gyre. Journal of Physical Oceanography 37, 2053–2080.
660 https://doi.org/10.1175/JPO3102.1
661 Zhou, X., Hess, A.V., Bu, K., Sagawa, T., Rosenthal, Y., 2022. Simultaneous Determination
662 of I/Ca and Other Elemental Ratios in Foraminifera: Comparing Results From Acidic
663 and Basic Solutions. Geochemistry, Geophysics, Geosystems 23, e2022GC010660.
664 https://doi.org/10.1029/2022GC010660
665
666

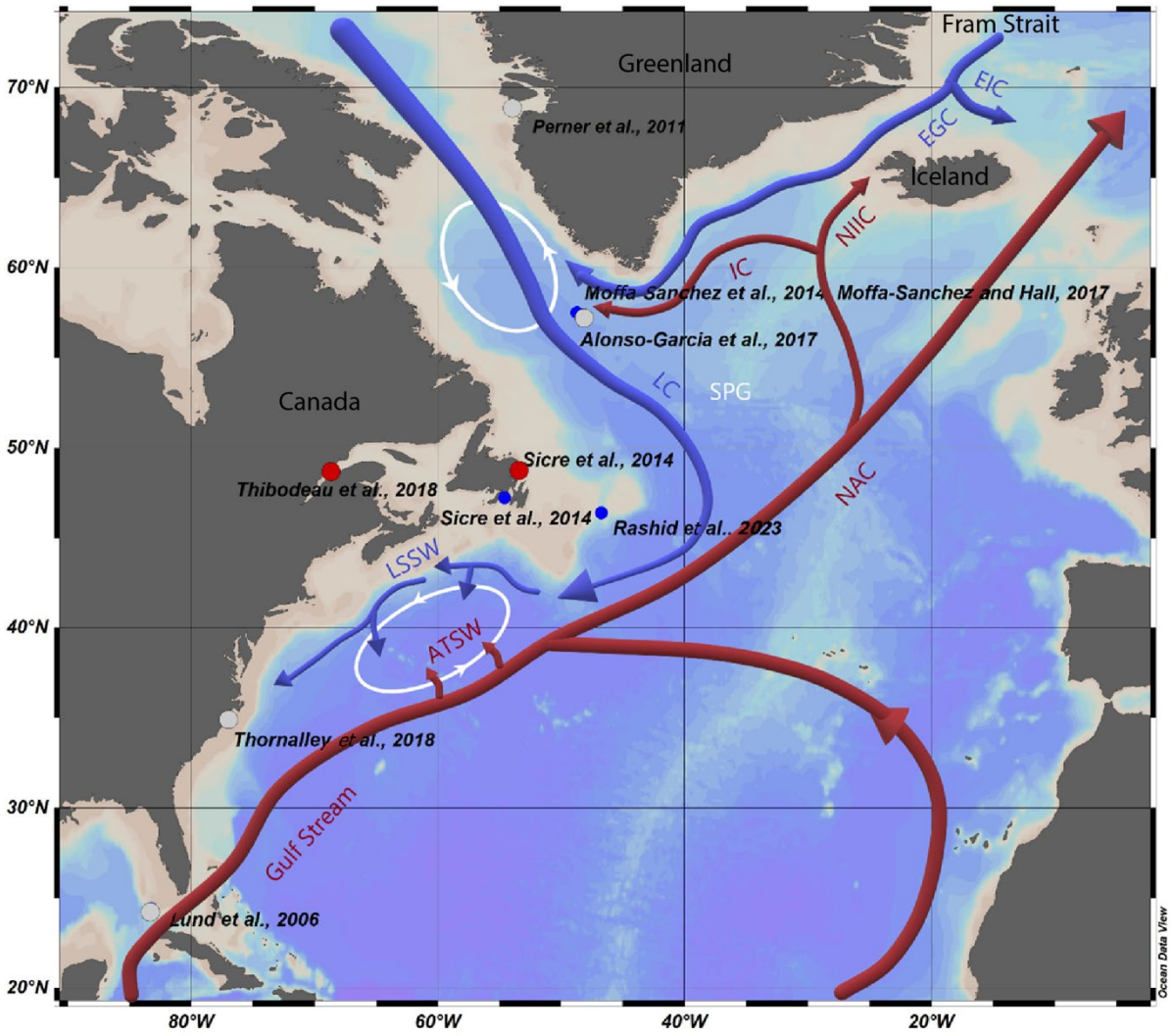

667

668 Figure 1 Map of the North Atlantic, ocean currents and locations of study cores listed in
669 Table 1. Red dots refer to studies indicating a warming during LIA, blue dots refer to studies
670 indicating a cooling during LIA, and grey dots refer to studies using non-temperature-related
671 proxies. Abbreviations on the map are: ATSW= Atlantic Temperate Slope Water; EIC= East
672 Iceland Current; EGC= East Greenland Current; IC= Irminger Current; LC= Labrador
673 Current; LSSW: Labrador Sea Slope Water; NAC= North Atlantic Current; NIIC= North
674 Iceland Irminger Current; SPG= sub-polar gyre; The two white circles indicate convection;
675 the upper one refers to Labrador Sea Convection while the lower one refers to Northern
676 Recirculation Gyre. Figure made with Ocean Data View (Schlitzer, 2018)

677
678

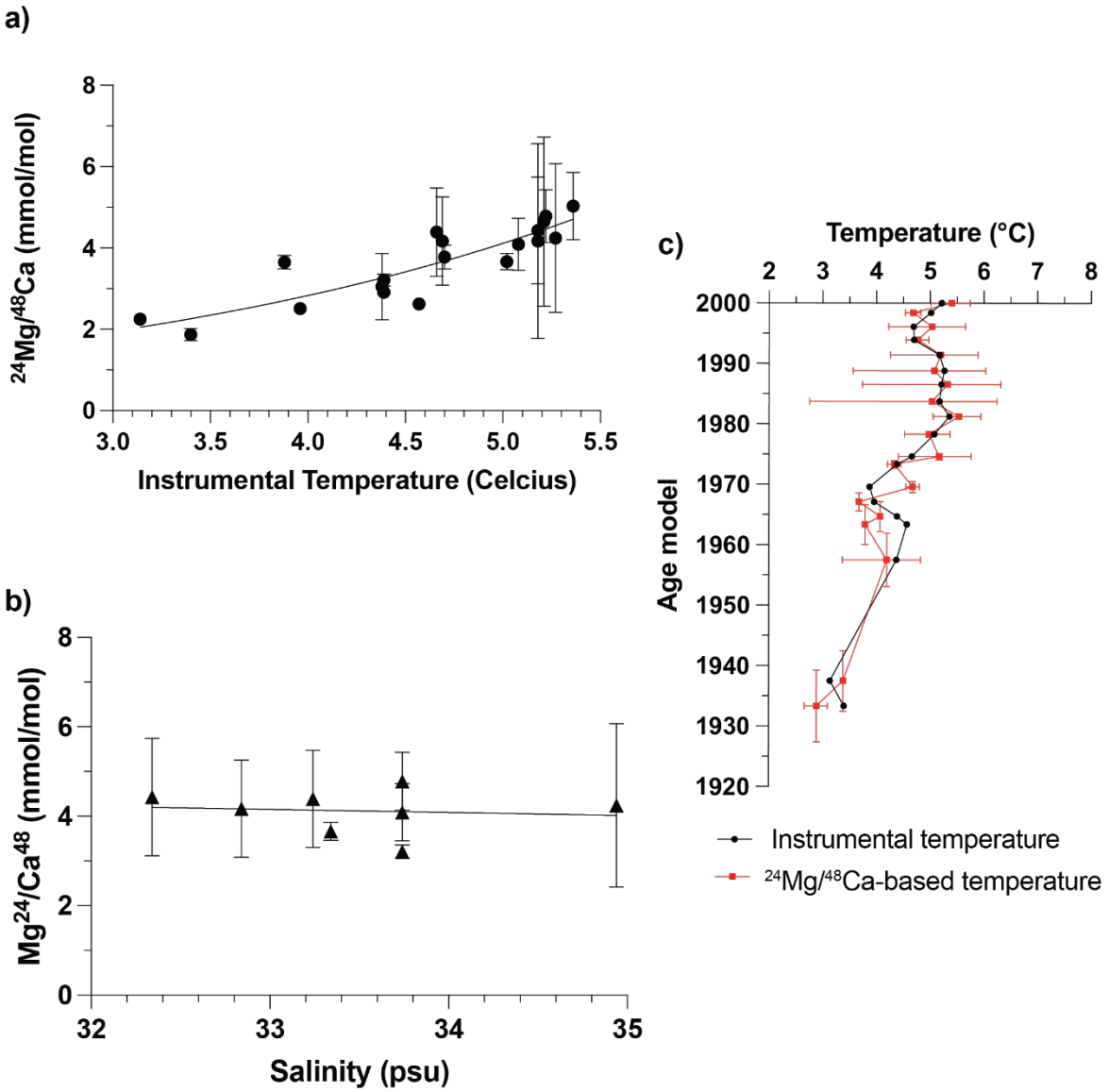

679
680 Figure 2 Best-fit curve for the MeRC-corrected $^{24}Mg/^{48}Ca$ data against a) instrumental temperature
681 and b) instrumental salinity, respectively. Error bars represent the standard deviation of replicate
682 measurements. In panel c) we plot instrumental temperature and reconstructed temperature from core
683 CR02-23 based on MeRC-corrected $^{24}Mg/^{48}Ca$ data best fit. Error bars represent standard deviation
684 from replication measurement (temperature, x-axis) and error from ^{210}Pb CRS-model (year, y-axis).

685

686

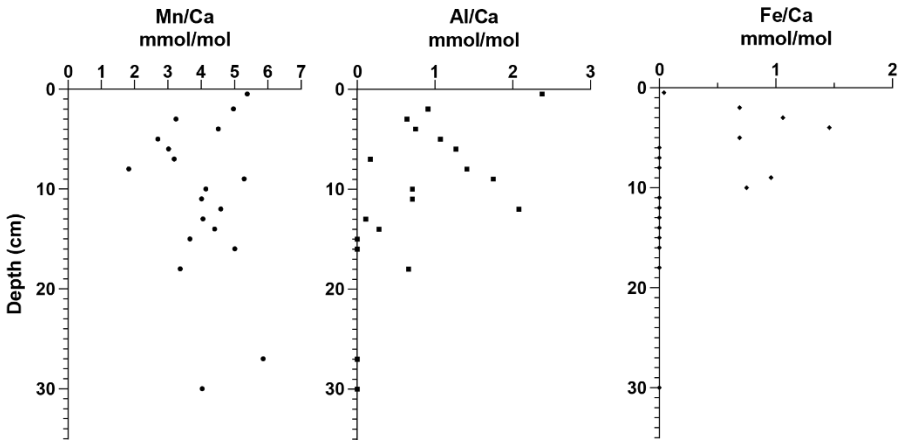

687

688 Figure 3 Ratio of contaminant (Mn, Al and Fe) on Ca downcore of CR02-23

689

690

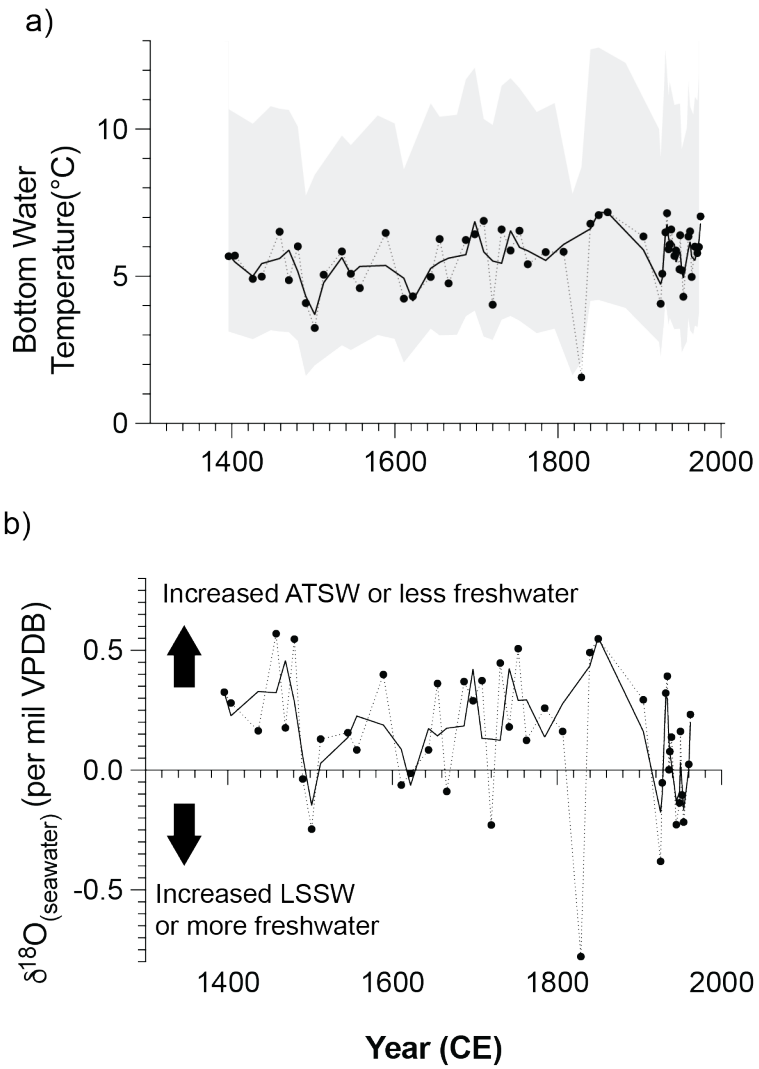

691
692

693 Figure 4. a) Bottom Water Temperature Reconstruction and b) seawater oxygen isotope
694 reconstruction of the St. Lawrence Estuary from 1396 to 1975 CE. The thick lines correspond
695 to a 3-point moving average. Temperature uncertainty was set at 95% of the confidence
696 interval of the equation fit of the 3-point moving average, excluding the outlier at 1829 CE.

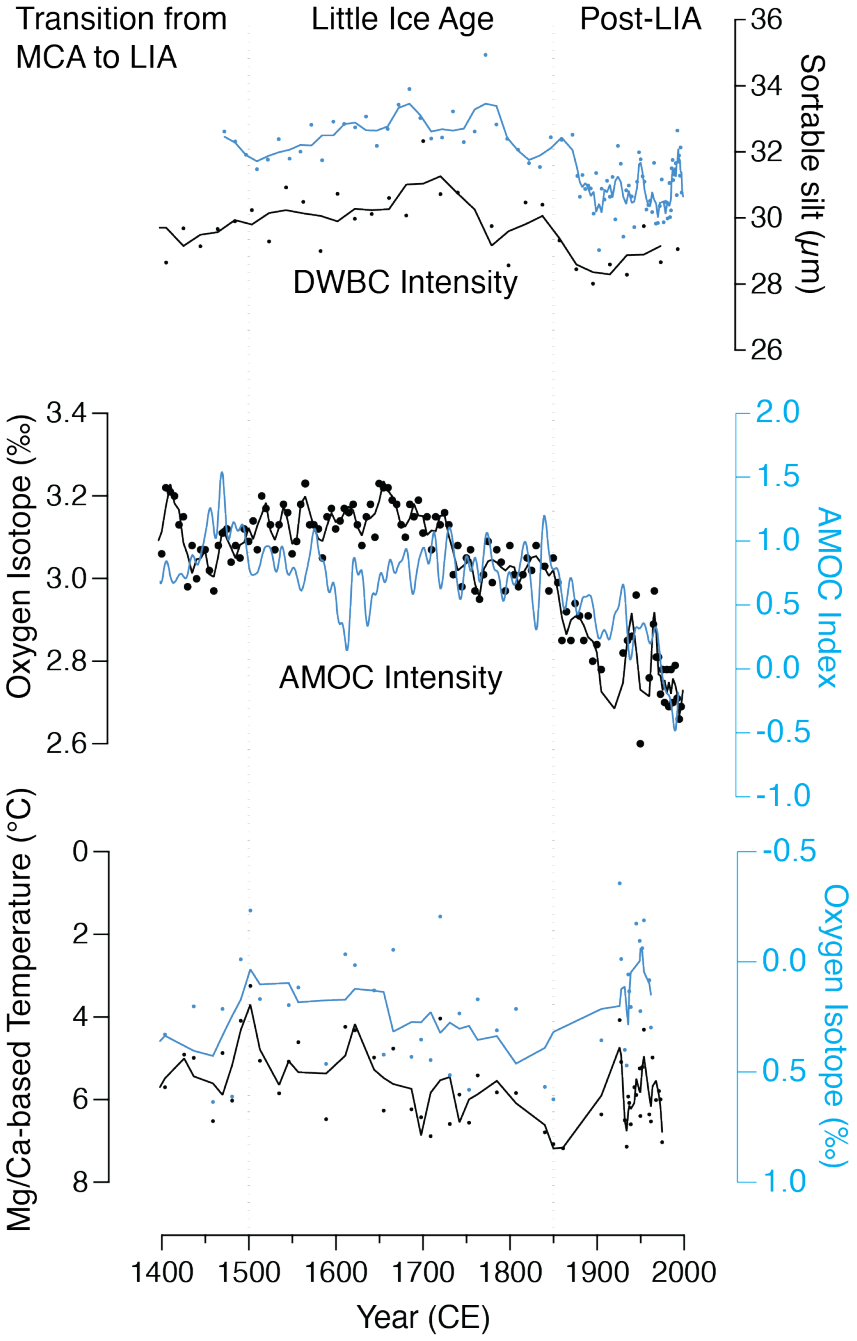

Figure 5 Comparison of selected LIA records with our result. Upper panel display sortable silt in core KNR-178-48JPC in blue KNR-178-56JPC in black which is used as a proxy of flow speed of deep western boundary current (Thornalley et al., 2018). Middle panel display AMOC index in blue (Rahmstorf et al. 2015) and $\delta^{18}O$ of *G. auriculata* in core MD99-2220 (Thibodeau et al., 2010, 2018). Bottom panel display bottom water reconstruction Mg/Ca of *G. auriculata* from core MD99-2220 (this study) in black and reconstructed seawater $\delta^{18}O$ (this study) in black. The black vertical dashed lines indicate the suggested separation between different time intervals.